

Article

Unsymmetrical Hexafluorocyclopentene-Linked Twisted π -Conjugated Molecules as Dual-State Emissive Luminophores [†]

Shigeyuki Yamada ^{1,*} , Akito Nishizawa ¹, Kazuki Kobayashi ¹, Keigo Yoshida ¹, Masato Morita ¹, Tomohiro Agou ² , Takaaki Hosoya ², Hiroki Fukumoto ²  and Tsutomu Konno ¹

¹ Faculty of Molecular Chemistry and Engineering, Kyoto Institute of Technology, Matsugasaki, Sakyo-ku, Kyoto 606-8585, Japan; m9673017@edu.kit.ac.jp (A.N.); b8151502@edu.kit.ac.jp (K.K.); b8151174@edu.kit.ac.jp (K.Y.); d9871006@edu.kit.ac.jp (M.M.); konno@kit.ac.jp (T.K.)

² Department of Quantum Beam Science, Graduate School of Science and Engineering, Ibaraki University, 4-12-1 Naka-Narusawa, Hitachi 316-8511, Japan; tomohiro.agou.mountain@vc.ibaraki.ac.jp (T.A.); takaaki.hosoya.th@vc.ibaraki.ac.jp (T.H.); hiroki.fukumoto.chem@vc.ibaraki.ac.jp (H.F.)

* Correspondence: syamada@kit.ac.jp; Tel.: +81-75-724-7517

[†] This paper is dedicated to the memory of Prof. Toshio Kubota, who passed away on 1 May 2020, for his valuable contribution to the chemistry of using octafluorocyclopentene.

Abstract: Dual-state emissive (DSE) luminophores, which can luminesce both in solution and in solid states, have recently attracted significant attention because of their broad applications. However, their development is difficult due to the difference in molecular design between solution- and solid-state luminophores. In this study, DSE luminophores based on unsymmetrical hexafluorocyclopentene-linked twisted π -conjugated structures carrying various substituents to tune the electron-density were designed and synthesized in a single-step reaction from heptafluorocyclopentene or perfluoro-1,2-diphenylcyclopentene derivatives. The twisted π -conjugated luminophores exhibited absorption in the UV region at approximately 330 nm, along with several signals in the high-energy region. Upon irradiating the luminophore solution (wavelength 330 nm), light-green to yellow photoluminescence (PL) was observed in the range of 422–471 nm with high PL efficiency. Theoretical calculations revealed that excitation from ground to excited states altered the structural shape of the luminophores from twisted to planar, leading to red-shifted PL and high PL efficiency (Φ_{PL}). The intense blue PL exhibited by the luminophores in the crystalline state was attributed to their twisted molecular structures that suppressed non-radiative deactivation via the effective blocking of π/π stacking interactions.

Keywords: π -conjugated molecules; dual-state emission; fluorine; twist; photoluminescence



Citation: Yamada, S.; Nishizawa, A.; Kobayashi, K.; Yoshida, K.; Morita, M.; Agou, T.; Hosoya, T.; Fukumoto, H.; Konno, T. Unsymmetrical Hexafluorocyclopentene-Linked Twisted π -Conjugated Molecules as Dual-State Emissive Luminophores. *Symmetry* **2021**, *13*, 1885. <https://doi.org/10.3390/sym13101885>

Academic Editor: György Keglevich

Received: 15 September 2021

Accepted: 28 September 2021

Published: 6 October 2021

Publisher's Note: MDPI stays neutral with regard to jurisdictional claims in published maps and institutional affiliations.



Copyright: © 2021 by the authors. Licensee MDPI, Basel, Switzerland. This article is an open access article distributed under the terms and conditions of the Creative Commons Attribution (CC BY) license (<https://creativecommons.org/licenses/by/4.0/>).

1. Introduction

Numerous luminescent substances exist that can be used in various applications, such as bioimaging probes [1,2], biosensors [2,3], light-emitting diodes [4–6], and lighting devices [4–6]. Luminescent materials can be divided into two classes according to the physical state of the luminophores: solution-state luminophores and solid-state luminophores. The former luminophores can be typically designed as extended π -conjugated planar structures, and their luminescence diminishes with the formation of molecular aggregates due to concentration quenching [7] or aggregation-caused quenching effects [8–10]. Meanwhile, the latter luminophores require special molecular design to enable the suppression of non-radiative deactivation by restricting molecular rotations or motions [11–13]. Despite difficulties in the design of versatile luminescent molecules, luminophores that luminesce in both solutions and solid states, called dual-state emissive (DSE) luminophores [14–17], have attracted considerable interest because of their broad applications in medicinal, biological,

and technological fields [18,19]. However, the development of DSE luminophores is difficult due to the distinct molecular design parameters. To date, reports on the molecular design of DSE luminophores have incorporated the following elements: (i) π -conjugation with a zero-twist donor-acceptor moiety to facilitate emission in solution state [20], (ii) twisted molecular structure to avoid fluorescence quenching in the solid state induced by π/π stacking, and (iii) a V-shaped configuration to enhance intramolecular charge transfer (ICT) and potentially suppress short-range π/π intermolecular interactions [21].

Our group has devoted intensive efforts to the development of efficient DSE luminophores based on the molecular design principles that facilitate the expression of DSE characteristics. It was reported that hexafluorocyclopentene derivatives bearing two donor-acceptor (D-A)-type fluorinated tolane arms in a symmetrical manner exhibited intense yellow fluorescence at a maximum photoluminescence (PL) wavelength (λ_{PL}) of 559 nm and PL efficiency (Φ_{PL}) of 0.75 when dissolved in CH_2Cl_2 . These luminophores also showed light-blue fluorescence ($\lambda_{\text{PL}} = 486 \text{ nm}$, $\Phi_{\text{PL}} = 0.43$) in their crystalline states (Figure 1a) [22].

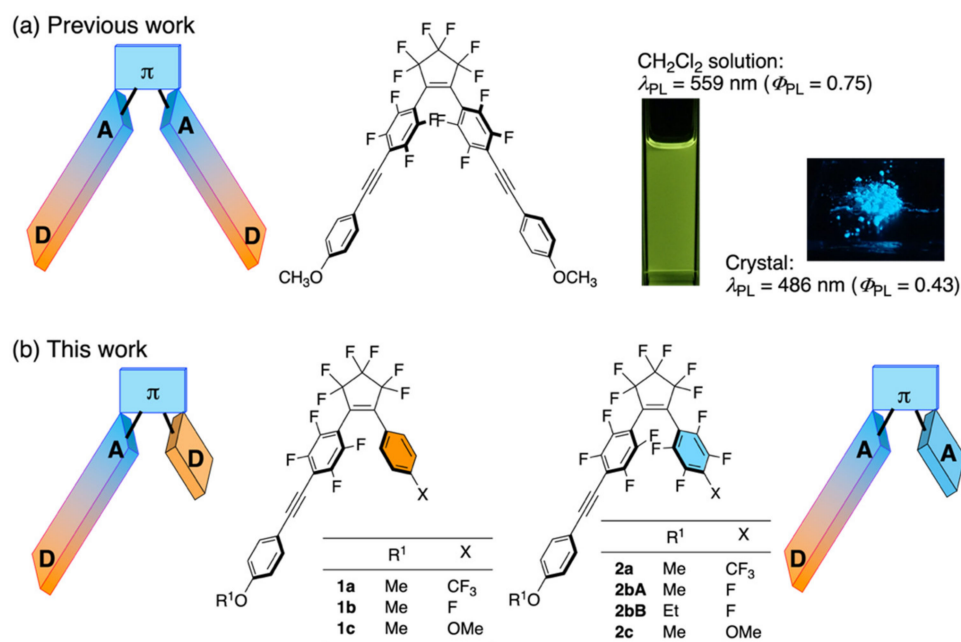


Figure 1. (a) Schematic illustration and molecular structure reported in our previous work; (b) Schematic illustrations and molecular structures **1** and **2** used in this work. D: donor; A: acceptor; π : π -conjugate structure.

In addition to the above molecular design, we envisioned that an unsymmetrical structural motif characterized by broken bilateral symmetry would not only exhibit increased solubility in common organic solvents and enhanced solution-phase PL intensity, but also show excellent crystalline-state PL properties owing to the suppression of ordered structure formation involving π/π stacking interactions. To demonstrate our molecular design for improved DSE luminophores, we designed and synthesized unsymmetrical hexafluorocyclopentene-linked twisted π -conjugated molecules, **1** and **2**, bearing both D-A type fluorinated tolane and benzene/multi-fluorinated benzene ring arms, and evaluated their photophysical behavior (Figure 1b). This paper presents the results of the theoretical molecular design and photophysical measurements in detail and discusses the photophysical characteristics of the developed luminophores based on theoretical calculations and molecular packing structures in the crystalline state.

2. Materials and Methods

2.1. General

High-resolution mass spectra (HRMS) were recorded on a JMS700MS spectrometer (JEOL, Tokyo, Japan) using the fast atom bombardment (FAB) method. Infrared (IR) spectra were recorded using the KBr method using an FTIR-4100 type A spectrometer (JASCO, Tokyo, Japan). All IR spectra are reported in wavenumber (cm^{-1}) units. ^1H nuclear magnetic resonance (NMR) (400 MHz) and ^{13}C NMR (100 MHz) spectra were acquired using an AVANCE III 400 NMR spectrometer (Bruker, Rheinstetten, Germany) in chloroform-*d* (CDCl_3) solution, and the chemical shifts were reported in parts per million (ppm) based on the residual protons or carbon in the NMR solvent. ^{19}F NMR (376 MHz) spectra were acquired using an AVANCE III 400 NMR spectrometer (Bruker, Rheinstetten, Germany) in CDCl_3 solution with CFCl_3 ($\delta_{\text{F}} = 0$ ppm) as an internal standard. All chemicals were of reagent grade and were purified by standard methods prior to use when necessary. The progress of the reactions was monitored via thin-layer chromatography (TLC), which was performed on silica gel TLC plates (Merck, Silica gel, 60F₂₅₄; Kenilworth, NJ, USA). Column chromatography was performed using silica gel (FUJIFILM Wako Pure Chemical Corporation, Wako-gel[®] 60N, 38–100 μm ; Osaka, Japan).

2.2. Materials

The unsymmetrical hexafluorocyclopentene-linked twisted π -conjugated molecules **1a–c** with a benzene ring and **2a–c** with a multi-fluorinated benzene ring in one arm, as shown in Figure 1, were synthesized from heptafluorocyclopentene derivatives or perfluoro-1,2-diphenylcyclopentene in a single-step reaction. The synthetic procedures and characterization of the compounds are described in the Supplementary Materials. The ^1H , ^{13}C , and ^{19}F -NMR spectra of **1a–c** and **2a–c** are demonstrated in Figures S2–S29, and their spectra proved that the compounds were of sufficient purity to enable evaluation of their photophysical behavior.

2.3. Single Crystal X-ray Diffraction

Single-crystal X-ray diffraction (XRD) was recorded on an XtaLAB AFC11 diffractometer (Rigaku, Tokyo, Japan). The reflection data were integrated, scaled, and averaged using CrysAlisPro (ver. 1.171.39.43a, Rigaku Corporation, Akishima, Japan) [23]. For empirical absorption corrections were utilized the SCALE 3 ABSPACK (CrysAlisPro). The crystal structures of the molecules were assigned using a SHELXT-2018/2 [24] and refined using a SHELXL-2018/3 [25], visualized using an Olex2 [26]. In the Cambridge Crystallographic Data Centre (CCDC) database were deposited the crystallographic data (CCDC 2,104,837 for **1c** and 2,104,836 for **2bB**). These data are accessible free of charge from the CCDC via www.ccdc.cam.ac.uk/data_request/cif (accessed on 30 September 2021).

2.4. DFT

Computations used in this study were carried out using the Gaussian 16 software package (Revision B.01) [27]. The optimized geometry was obtained from the calculation using the CAM-B3LYP hybrid functional [28,29] and the 6-31G(d) basis set with a conductor-like polarizable continuum solvation model (CPCM [30–32]) for CH_2Cl_2 . The theoretical excitation energies and dipole moments were calculated using time-dependent self-consistent field approximation [33,34] at the same level of theory.

2.5. Photophysical Property

Ultraviolet-visible (UV–vis) absorption spectra were recorded using a V-500 absorption spectrometer (JASCO, Tokyo, Japan). The PL spectra of the solution and crystal forms were acquired using an FP-6600 fluorescence spectrometer (JASCO, Tokyo, Japan). The absolute quantum yields in both the solution and crystalline phases were measured using a Quantaurus-QY measurement system C11347-01 (Hamamatsu Photonics, Hamamatsu,

Japan). PL lifetime measurement was carried out using a Quantaaurus-Tau fluorescence lifetime spectrometer C11367-34 (Hamamatsu Photonics, Hamamatsu, Japan).

3. Results and Discussion

3.1. Theoretical Assessment

Our study was initiated with a theoretical assessment of the designed unsymmetrical hexafluorocyclopentene-linked twisted π -conjugated molecules, using the Gaussian16 software. The optimized geometries of **1a–c** and **2a–c** were calculated using density functional theory (DFT) at the CAM-B3LYP/6-311++G(d,p)/CAM-B3LYP/6-31G(d) level of theory with CPCM for CH_2Cl_2 . The theoretical vertical transitions from the ground (S_0) to the excited (S_n) states were assessed using time-dependent (TD)-DFT calculations using the same functional and basis set. Figure 2 presents the calculated results, viz., optimized geometries, the highest occupied molecular orbital (HOMO), and the lowest unoccupied molecular orbital (LUMO) distributions at both the S_0 and S_1 states of **1a** with a CF_3 substituent in the aromatic ring opposite to the D-A type fluorinated tolane scaffold. The results for the other compounds, **1b**, **1c** and **2a–c**, are summarized in the Supplementary Materials (Figures S30 and S31 and Tables S1–S16).

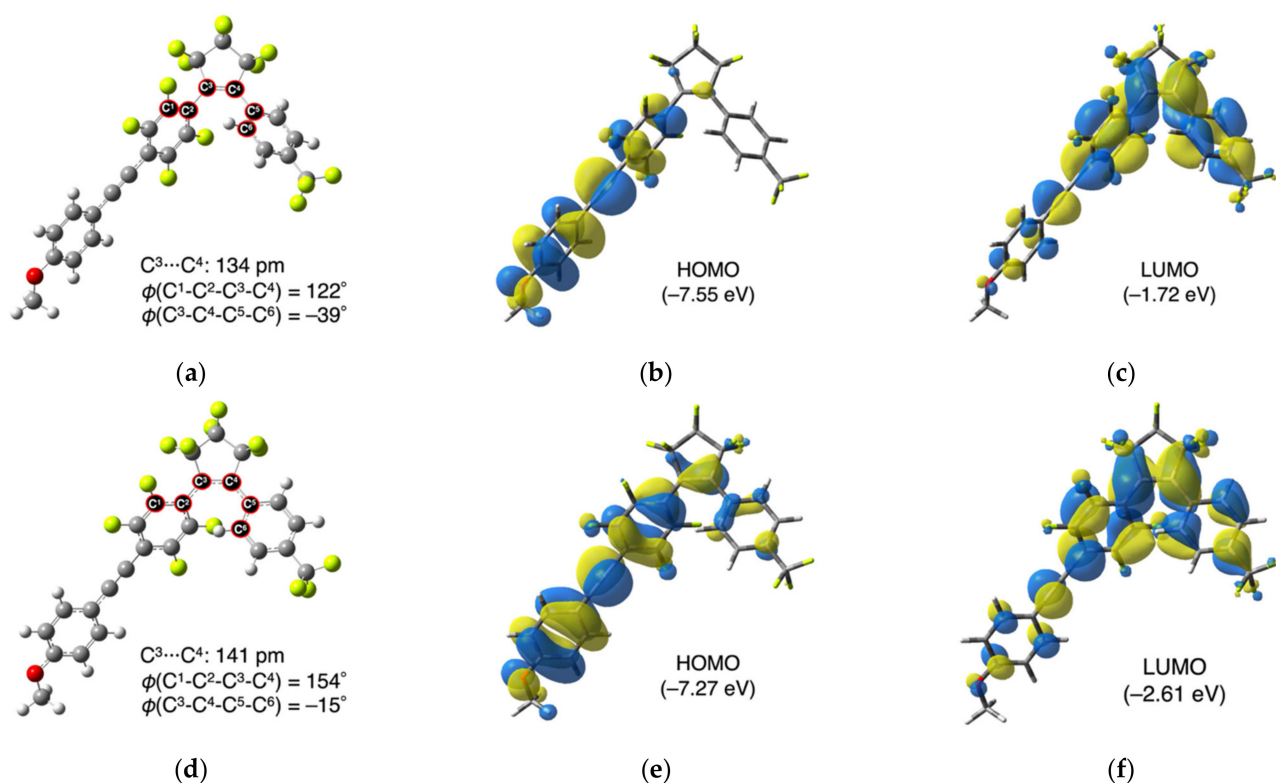


Figure 2. (a) Optimized geometry of **1a** in the ground S_0 state; (b) HOMO and (c) LUMO distributions of **1a** in S_0 state; (d) Optimized geometry of **1a** at the excited S_1 state; (e) HOMO and (f) LUMO distributions of **1a** at the S_1 state.

According to the geometry optimization results of **1a** in the S_0 state, it formed a twisted molecular configuration between the central hexafluorocyclopentene core and both aromatic arms, in which the dihedral angles made by $\text{C}^1\text{-C}^2\text{-C}^3\text{-C}^4$ and $\text{C}^3\text{-C}^4\text{-C}^5\text{-C}^6$, viz., $\phi(\text{C}^1\text{-C}^2\text{-C}^3\text{-C}^4)$ and $\phi(\text{C}^3\text{-C}^4\text{-C}^5\text{-C}^6)$, were 122° and -39° , respectively (Figure 2a). According to the electronic structure of **1a** in the S_0 state, the HOMO (-7.55 eV) lobe existed over the D-A type fluorinated tolane-arm (Figure 2b), whereas the LUMO (-1.72 eV) lobe was primarily localized over the twisted diarylethene moiety (Figure 2c). Interestingly, the optimized geometry at the S_1 state was altered to reduce the twisted structure to a planar structure with increasing $\text{C}^3\cdots\text{C}^4$ double bond length: $\phi(\text{C}^1\text{-C}^2\text{-C}^3\text{-C}^4)$ and $\phi(\text{C}^3\text{-C}^4\text{-C}^5\text{-C}^6)$ were 154° and -15° , respectively (Figure 2d). The increasing structural planarity in the

S_1 state slightly spread the HOMO and LUMO lobes throughout the π -conjugated unit in the molecule, which led to an increase in the HOMO energy level of -7.27 eV and a decrease in the LUMO energy level of -2.61 eV. This resulted in a small HOMO-LUMO energy gap (ΔE^{H-L}) of 4.66 eV. The electronic orbital distributions between the HOMO and LUMO in the S_1 state promote ICT to radiatively deactivate excitons via the ICT excited state. Considering the structural and electronic alterations between the S_0 and S_1 states, the unsymmetrical twisted π -conjugated molecules can be anticipated to exhibit luminescence both in solution and solid states. Therefore, the proposed molecular design is suitable for the rational development of efficient DSE luminophores.

3.2. Crystal Structures of **1c** and **2bB**

After validation of the proposed molecular design for DSE luminophores using theoretical studies, the unsymmetrical hexafluorocyclopentene-linked twisted π -conjugated compounds **1a–c** with a benzene ring arm and **2a–c** with a multi-fluorinated benzene ring-arm were synthesized, and the synthetic protocols are illustrated in Figure S1. The structurally pure compounds were obtained via double isolation techniques of column chromatography (eluent: hexane/EtOAc = 15/1) and recrystallization from $\text{CH}_2\text{Cl}_2/\text{MeOH}$ ($v/v = 1/1$). Suitable structural assessments, such as ^1H , ^{19}F , and ^{13}C NMR, IR, and HRMS, proved that the synthesized compounds were of sufficient purity to enable evaluation of their photophysical characteristics. Among the synthesized compounds, **1c** with a 4-methoxyphenyl arm and **2bB** with a pentafluorophenyl arm furnished single crystals suitable for X-ray crystallographic analysis. Figure 3 shows the crystal structures of **1c** and **2bB**.

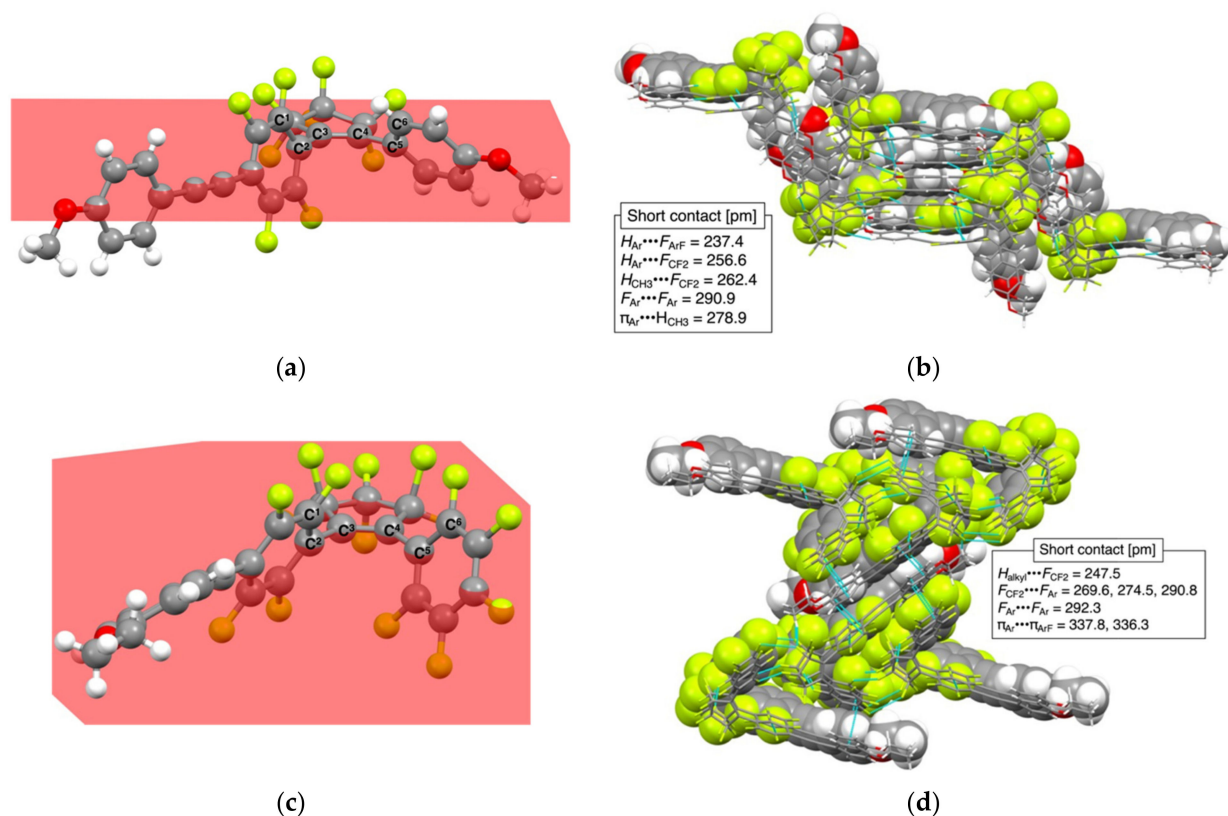


Figure 3. Crystal structure of (a) **1c** and (c) **2bB**. The plane comprising four atoms, $\text{C}^2\text{-C}^3\text{-C}^4\text{-C}^5$, is colored red. Packing structures of (b) **1c** and (d) **2bB**. The blue line denotes short contact distance of less than the sum of two atomic van der Waals radii.

Furthermore, **1c** belongs to the monoclinic crystalline system in the $P 1 2_1/c 1$ space group ($Z = 4$). The actual dihedral angles, that is, $\phi(C^1-C^2-C^3-C^4)$ and $\phi(C^3-C^4-C^5-C^6)$, were observed to be 111° and -51° , respectively, indicating a twisted structure, which was in parity with the theoretically optimized geometry. The packing structures were formed with several intermolecular interactions, such as H \cdots F hydrogen bonding (short-distance atomic contact: 237.4 pm for $H_{Ar}\cdots F_{ArF}$, 256.6 pm for $H_{Ar}\cdots F_{CF2}$, 262.4 pm for $H_{CH3}\cdots F_{CF2}$), F \cdots F interactions (290.9 pm for $F_{Ar}\cdots F_{Ar}$), and CH \cdots π interactions (278.9 pm for $C_{Ar}\cdots H_{CH3}$), in which the short-distance atomic contacts were less than the sum of the van der Waals radii of two atoms (H: 120 pm, C: 170 pm and F: 147 pm) [35]. However, **2bB** crystallized in an orthorhombic crystalline system belonging to the $P 2_1 2_1 2_1$ space group, and four molecular units of **2bB** were included in a unit cell. The central hexafluorocyclopentene core was sharply twisted with respect to both the fluorinated tolane and multi-fluorinated benzene ring arms, in which the dihedral angles $\phi(C^1-C^2-C^3-C^4)$ and $\phi(C^3-C^4-C^5-C^6)$, were 66° and -117° , respectively. The packing structures constituted several intermolecular interactions. Short-distance contacts, such as H \cdots F hydrogen bonding (247.5 pm for $F_{CF2}\cdots H_{alkyl}$), F \cdots F interactions (269.6 pm, 274.5 pm, and 290.8 pm for $F_{CF2}\cdots F_{Ar}$; 292.3 pm for $F_{Ar}\cdots F_{Ar}$), and electrostatic $\pi\cdots\pi$ interactions (337.8 pm and 336.3 pm for $C_{Ar}\cdots C_{Ar-F}$), were observed. The unsymmetrical twisted structural shape can be attributed to the avoidance of intermolecular π/π stacking via orbital overlap throughout the π -conjugated unit in the molecule. Therefore, the unsymmetrical twisted molecules were expected to exhibit PL in crystalline states.

3.3. Photophysical Measurements in Solution State

We first investigated the photophysical behavior of the hexafluorocyclopentene-linked twisted π -conjugated molecules **1a–c** and **2a–c**, in a dilute solution state. The sample was prepared by dissolving in CH_2Cl_2 , and the concentration was adjusted to 1×10^{-5} mol L^{-1} for UV–vis absorption measurements and 1×10^{-6} mol L^{-1} for PL measurements. Figure 4 shows the UV–vis absorption and PL spectra, and the chromaticity diagram for PL color as defined by the Commission Internationale de l’Eclairage (CIE). Table 1 summarizes the obtained photophysical data.

Hexafluorocyclopentene-linked twisted π -conjugated molecules **1a–c** bearing a benzene ring arm absorbed UV light and showed similar absorption spectra with several absorption bands (Figure 4a). **1a** with a 4-(trifluoromethyl)phenyl arm when dissolved in CH_2Cl_2 displayed two absorption bands with maximum absorption wavelengths (λ_{abs}) of approximately 331 and 257 nm, along with a shoulder signal at approximately 315 nm. Through TD-DFT calculations, the two intense absorption bands observed were assigned to two $\pi\text{-}\pi^*$ transitions involving HOMO \rightarrow LUMO for the low-energy absorption band and HOMO \rightarrow LUMO+1 for the high-energy absorption band (Figure S31 and Table S3). Further, **1b** with a 4-fluorophenyl arm showed similar absorption behavior to **1a**, while **1c** with a 4-methoxyphenyl arm displayed not only the two intense absorption bands with λ_{abs} at approximately 328 and 261 nm, but also an absorption band with λ_{abs} at approximately 300 nm. The corresponding transitions were $\pi\text{-}\pi^*$ transitions involving HOMO \rightarrow LUMO and HOMO–1 \rightarrow LUMO for the long- and short-wavelength absorption bands, respectively.

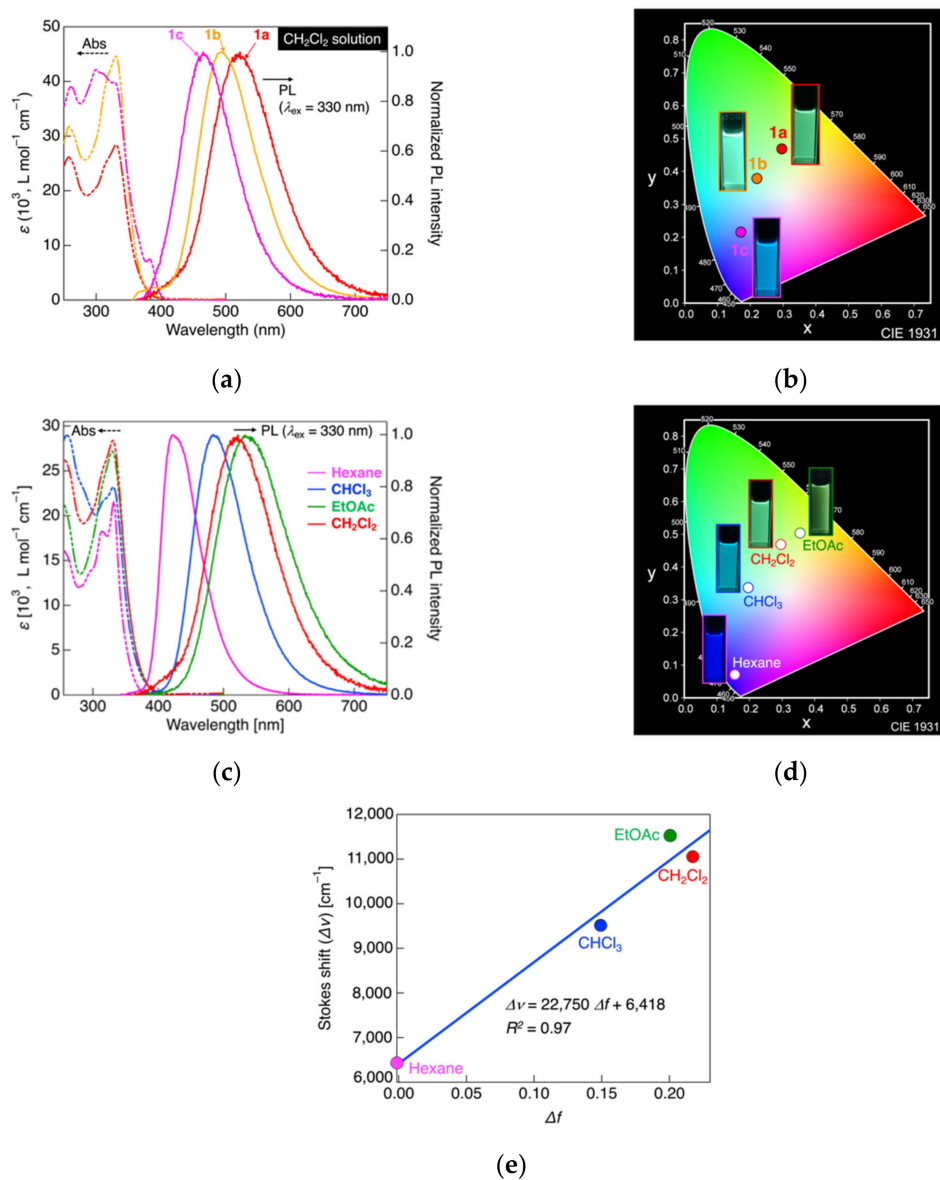


Figure 4. (a) UV-vis absorption spectra (1×10^{-5} mol L⁻¹) and PL spectra (1×10^{-6} mol L⁻¹) in CH₂Cl₂ for **1a–c**; (b) Photographs of PL under UV irradiation ($\lambda_{\text{ex}} = 365$ nm) and CIE chromaticity diagram of PL for **1a–c**; (c) UV-vis absorption and PL spectra of **1a** in different solvents; (d) PL color of **1a** in various solvents under UV irradiation ($\lambda_{\text{ex}} = 365$ nm) and the color diagram defined by CIE; (e) Lippert–Mataga plot obtained from the relationship between Stokes shift and solvent parameter. R^2 indicates coefficient of determination.

Table 1. Photophysical data for **1a–c** recorded in various solvents¹.

Molecule	Solvent	λ_{abs} [ϵ (10 ³ , L mol ⁻¹ cm ⁻¹)] ²	λ_{PL} (Φ_{PL}) ³	CIE Coordinate (x, y)
1a	CH ₂ Cl ₂	257 [25.5], 315sh [39.8], 331 [27.7]	522 (0.99)	(0.3, 0.47)
	Hexane	255 [16.1], 315 [18.2], 332 [21.6]	422 (0.7)	(0.16, 0.07)
	CHCl ₃	260 [28.9], 316sh [21.7], 331 [23.2]	438 (0.94)	(0.2, 0.34)
	EtOAc	256 [21.1], 314sh [23.3], 330 [27.2]	534 (0.55)	(0.36, 0.5)
1b	CH ₂ Cl ₂	259 [30.1], 314sh [24.9], 332 [42.8]	402sh, 493 (0.90)	(0.22, 0.38)
1c	CH ₂ Cl ₂	261 [38.6], 300 [41.9], 311sh [41.4], 328 [39.9]	465 (0.57)	(0.17, 0.22)

¹ Concentration: 1×10^{-5} mol L⁻¹ for UV-vis absorption measurements and 1×10^{-6} mol L⁻¹ for PL measurements. ² ϵ : molar extinction coefficient; sh: shoulder peak. ³ Measured using an integrating sphere.

The PL behaviors of **1a–c** in CH₂Cl₂ solution were examined at an excitation wavelength (λ_{ex}) of 330 nm. **1a**, which had a 4-(trifluoromethyl)phenyl arm, showed a single PL band with a maximum PL wavelength (λ_{PL}) of approximately 522 nm and high PL efficiency ($\Phi_{\text{PL}} = 0.99$). **1a** dissolved in CH₂Cl₂ was observed to emit yellowish-green PL with coordinates (x, y) = (0.3, 0.47) according to the PL color and CIE chromaticity diagram (Figure 4b). When the luminescence decay profiles were measured to reveal the luminescence process, the luminescence lifetime (τ) was found to be 3.6 nano-second (ns), indicating that PL of **1a** is fluorescence (Figure S33 and Table S18). **1b** with a 4-fluorophenyl arm and **1c** with a 4-methoxyphenyl arm exhibited single PL bands at λ_{PL} of approximately 493 and 465 nm, respectively, with a moderate to high Φ_{PL} , upon excitation at 330 nm. Their luminescence process was also concluded to be fluorescence because of the nano-second order of τ (2.9 ns for **1b** and 1.9 ns for **1c**). The PL color was bluish-green with coordinates of (0.22, 0.38) for **1b** and blue with coordinates of (0.17, 0.22) for **1c**. The λ_{PL} shift observed upon modulating the substituent at the 4-position of the benzene ring arm can be rationalized by the HOMO-LUMO energy gap ($\Delta E^{\text{H-L}}$) of the S₁ state: the $\Delta E^{\text{H-L}}$ of the S₁ states were 4.66, 4.76, and 4.75 eV for **1a**, **1b** and **1c**, respectively.

This indicates that the CF₃ group at the 4-position of the benzene ring arm in **1a** causes a decrease in $\Delta E^{\text{H-L}}$ through a significant reduction in the LUMO energy level, resulting in the emission of long-wavelength PL. Meanwhile, the electron-donating substituents in **1b** and **1c** increase the HOMO energy level via the resonance effect, which increases the $\Delta E^{\text{H-L}}$ and results in high-energy emission with a short λ_{PL} .

Figure 4c presents the UV-vis absorption and PL spectra of **1a** in various solvents, such as hexane, chloroform (CHCl₃), and ethyl acetate (EtOAc). The solvent polarity can be determined from the relative dielectric constant at 25 °C: hexane (1.88) < CHCl₃ (4.81) < EtOAc (6.02) < CH₂Cl₂ (8.93). Table 1 summarizes the photophysical data. The absorption spectra of **1a** in different solvents were almost consistent and independent of the solvent polarity, whereas the PL band shifted upon changing the solvent polarity. Thus, **1a** in the less polar hexane solution emitted deep blue PL with coordinates of (0.16, 0.07) with a λ_{PL} at approximately 422 nm. Upon increasing the solvent polarity based on the relative dielectric constant, the λ_{PL} was found to be red-shifted, resulting in light-blue PL with coordinates of (0.20, 0.34) in CHCl₃, yellowish-green PL (0.30, 0.47) in CH₂Cl₂, and yellow PL in EtOAc (0.36, 0.50). Based on the effect of solvents on the photophysical properties, we created a Lippert–Mataga plot [36,37] with a solvent polarity parameter (Δf) on the horizontal axis and the Stokes shift ($\Delta\nu = \nu_{\text{abs}} - \nu_{\text{PL}}$) on the vertical axis (Figure 4e), which was used to determine the dipole moments of the molecules in the excited states. With a least-squares approximation, a linear relationship between $\Delta\nu$ and Δf was found, as expressed in Equation (1):

$$\Delta\nu = 22,750 \Delta f + 6418, \quad (1)$$

The slope of this equation correlates strongly with the difference in the dipole moments between the excited and ground states: $\Delta\mu = \mu_{\text{e}} - \mu_{\text{g}}$, where μ_{e} and μ_{g} represents the dipole moments in the excited and ground states, respectively. A large $\Delta\mu$ value of 24.8 D was obtained for **1a**, which clearly indicated that the PL of **1a** was due to radiative deactivation of the CT excited state via ICT transition [37]. The major PL bands of **1b** and **1c** also result from radiative deactivation via ICT transition.

Subsequently, we examined the solution state photophysical behavior of **2a–c** with a multi-fluorinated benzene ring arm. Figure 5 shows the corresponding UV-vis absorption and PL spectra and the CIE color diagram for PL, and Table 2 summarizes the photophysical data.

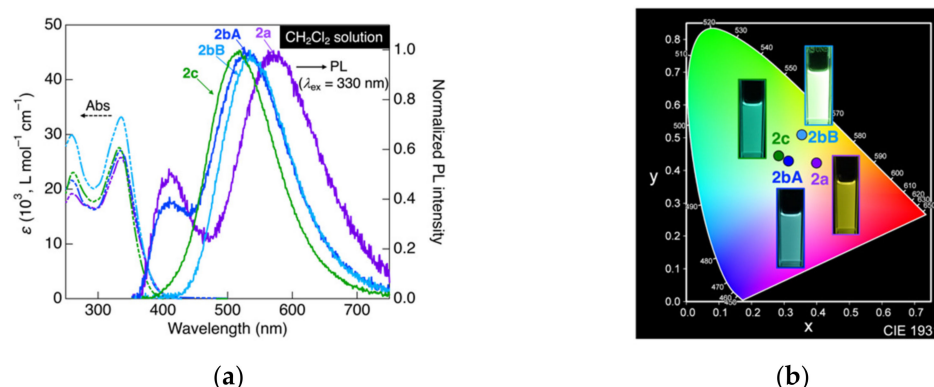


Figure 5. (a) UV-vis absorption ($1 \times 10^{-5} \text{ mol L}^{-1}$) and PL ($1 \times 10^{-6} \text{ mol L}^{-1}$) spectra in CH_2Cl_2 for **2a–c**; (b) Photographs of PL under UV irradiation ($\lambda_{\text{ex}} = 365 \text{ nm}$) and CIE chromaticity diagram of PL for **2a–c**.

Table 2. Photophysical data for **2a–c** recorded in CH_2Cl_2 solvent ¹.

Molecule	λ_{abs} [ϵ ($10^3, \text{L mol}^{-1} \text{cm}^{-1}$)] ²	λ_{PL} (Φ_{PL}) ³	CIE Coordinate (x, y)
2a	259 [19.2], 335 [25.8]	409, 571 (0.35)	(0.4, 0.42)
2bA	259 [21.6], 334 [27.1]	410, 533 (0.78)	(0.31, 0.43)
2bB	259 [29.9], 336 [33.2]	535 (0.26)	(0.35, 0.51)
2c	261 [23.0], 332 [27.6]	518 (0.88)	(0.28, 0.44)

¹ Concentration: $1.0 \times 10^{-5} \text{ mol L}^{-1}$ for the UV-vis absorption measurements and $1.0 \times 10^{-6} \text{ mol L}^{-1}$ for the PL measurements. ² ϵ : Molar extinction coefficient. ³ Measured using an integrating sphere.

In UV-vis absorption measurements, two absorption bands were observed in the UV region at λ_{abs} 332–336 nm and 259–261 nm (Figure 5a, left axis). TD-DFT calculations revealed that the low-energy absorption band originated from the $\pi\text{-}\pi^*$ transition involving HOMO \rightarrow LUMO, whereas it was calculated that the higher absorption bands were involved in the vertical transitions from HOMO to LUMO+1 for **2a** and **2b** and HOMO-1 to LUMO for **2c**. Upon irradiation of the CH_2Cl_2 solutions of **2a–c** with UV light ($\lambda_{\text{ex}} = 330 \text{ nm}$), PL was observed with a Φ_{PL} value in a range of 0.26–0.88. The PL of **2a–c** was also assigned as fluorescence resulting from the nano-second order lifetime (Figure S33). In contrast to the PL characteristics of **1a–c**, **2a** and **2bA** exhibited two PL bands at approximately 409–410 nm and a longer-wavelength region ($\lambda_{\text{PL}} = 571 \text{ nm}$ for **2a** and 533 nm for **2bA**). However, the other two analogues, viz., **2bB** and **2c**, exhibited single PL bands at approximately 535 nm (**2bB**) and 518 nm (**2c**) (Figure 5a, right axis), respectively. According to the above discussions and our previous report [22], the major PL band in the longer-wavelength region can be assigned to radiative deactivation via ICT transition. Additionally, the minor PL band observed in the cases of **2a** and **2bA** in the range of 409–410 nm can be assigned to radiative deactivation from locally excited (LE) states. The lifetime measurement in the high-energy PL band for **2a** and **2bA** was found to be fitted with the second-order fluorescence decay curve including short-period lifetime (Figure S33), which can support the assignment of the high-energy PL as radiative deactivation from the LE states. The PL color of **2a–c** varied between yellow and green (Figure 5b). Similar to the PL behavior of **1a–c**, λ_{PL} of **2a–c** underwent a gradual blue-shift with the alteration of the terminal substituent in the order: $\text{CF}_3 \rightarrow \text{F} \rightarrow \text{OCH}_3$ due to increase in the $\Delta E^{\text{H-L}}$ of the S_1 state (4.44, 4.58, and 4.63 eV for **2a**, **2b**, and **2c**, respectively) (Table S1). Accordingly, the photophysical properties of the synthesized unsymmetrical hexafluorocyclopentene-linked twisted π -conjugated molecules were similar to those of symmetrical molecules in solution. However, a slight decrease in Φ_{PL} was observed due to the shortened π -conjugation length.

3.4. Crystalline-State Photoluminescence Behavior

Next, we tested the crystalline-state PL behavior of the unsymmetrical hexafluorocyclopentene-linked twisted π -conjugated molecules, **1a–c** and **2a–c**. Figure 6 illustrates the PL spectra of **1a–c** and **2a–c** in the crystalline state upon irradiation with light of wavelength 300 nm (λ_{ex}), photographs under UV irradiation ($\lambda_{\text{ex}} = 365$ nm), and CIE color diagram of the PL. The photophysical data obtained are summarized in Table 3.

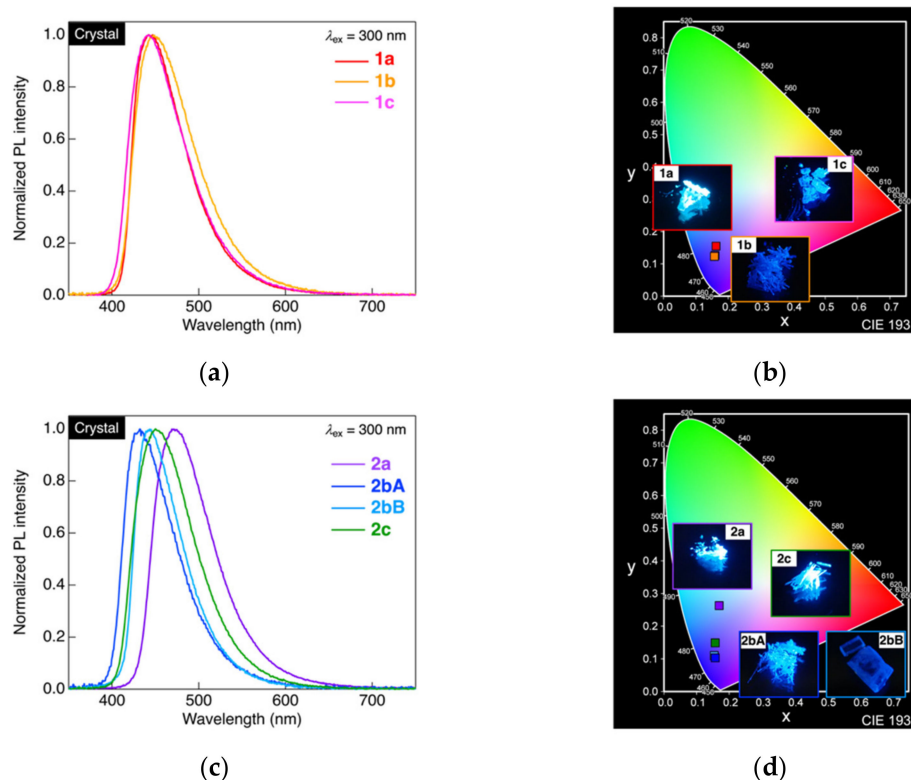


Figure 6. (a) PL spectra of **1a–c** in crystalline form ($\lambda_{\text{ex}} = 300$ nm); (b) photographs of **1a–c** under UV irradiation and their CIE color diagram; (c) PL spectra of **2a–c** in crystalline form ($\lambda_{\text{ex}} = 300$ nm); (d) photographs of **2a–c** under UV irradiation and their CIE color diagram.

Table 3. Photophysical data of **1a–c** and **2a–c** in the crystalline state.

Molecule	λ_{PL}^1	Φ_{PL}^2	CIE Coordinate (x, y)
1a	449	0.98	(0.16, 0.16)
1b	443	1.0	(0.16, 0.12)
1c	443	1.0	(0.16, 0.13)
2a	471	1.0	(0.17, 0.26)
2bA	432	0.52	(0.16, 0.1)
2bB	443	0.99	(0.15, 0.11)
2c	450	1.0	(0.16, 0.15)

¹ Excitation wavelength: 300 nm. ² Measured using an integrated sphere.

A single PL band at approximately 449 nm was observed for **1a**, and the corresponding PL color was blue with coordinates of (0.16, 0.16). It was revealed that the PL was assigned as fluorescence from the lifetime measurement (Figure S36) and, to our delight, the Φ_{PL} was as high as 0.98 in the crystalline state. A similar blue PL with a single PL band at approximately 443 nm was observed for **1b** and **1c** with high Φ_{PL} (up to 1.0). Single crystal X-ray studies performed on **1c** (Figure 3) indicated the formation of rigid structures owing to the contribution of H \cdots F hydrogen bonds and CH/ π interactions, and not π/π

stacking, which is likely responsible for the significant retardation of the non-radiative rate constant owing to suppression of molecular motions, like rotation, leading to high Φ_{PL} (up to 1.0). In addition, the compounds **2a–c** exhibited blue or light-blue PL with a λ_{PL} at approximately 432–471 nm and a high Φ_{PL} in the range 0.52–1.0 in the crystalline state. Compared with the PL behavior in dilute solution, the λ_{PL} in the crystalline state was significantly blue shifted by 20–100 nm. The high-energy PL in the crystalline state is attributable to radiative deactivation through locally excited (LE) states due to the twisted molecular structure, which shortens the effective π -conjugation length. Therefore, the twisted structural shape effectively avoids non-radiative deactivation due to the absence of π/π stacking interactions, resulting in highly efficient PL behavior in the crystalline state.

4. Conclusions

We designed and synthesized unsymmetrical hexafluorocyclopentene-linked twisted π -conjugated molecules bearing both D-A type fluorinated tolane and aromatic ring arms as efficient DSE luminophores. The prepared DSE luminophores were emissive in the solution state, and their electronic properties were strongly influenced by terminal molecular substituents. Theoretical investigations using TD-DFT calculations indicated that the twisted structures were transformed to planar molecular shapes in the excited states. It is postulated that this structural change promoted ICT, resulting in yellow PL from ICT excited states. The unsymmetrical twisted π -conjugated molecules also exhibited high PL efficiency (Φ_{PL} up to 1.0) with blue PL color in the crystalline state due to the effective inhibition of π/π stacking interactions by the twisted molecular shapes. These observations indicate that the prepared luminophores represent promising molecular designs that can potentially benefit the development of improved DSE luminophores. Further investigation is ongoing in our research group.

Supplementary Materials: The following are available online at <https://www.mdpi.com/article/10.3390/sym13101885/s1>, Figure S1: Synthetic scheme, Figures S2–S29: NMR spectra, Figure S30: Optimized geometry, Figure S31: HOMO and LUMO diagrams, Figure S32: UV–vis and PL spectra in CH_2Cl_2 solution, Figure S33: Fluorescence decay profiles in CH_2Cl_2 solution, Figure S34: Solvent effect of photophysical property for **1a**, Figure S35: Excitation and PL spectra in crystalline state, Figure S36: Fluorescence decay profiles in crystalline state, Table S1: Structural and electronic parameters obtained from DFT calculation, Table S2: Energy and dipole moment calculated from DFT calculation, Tables S3 and S4: Theoretical transition calculated by TD-DFT calculation, Tables S5–S16: Cartesian coordinate, Table S17: Crystallographic data, Table S18: Average fluorescence lifetime in CH_2Cl_2 solution, Table S19: Photophysical data of **1a** in various solvents, Table S20: Average fluorescence lifetime in crystalline state.

Author Contributions: Conceptualization, S.Y.; methodology, S.Y.; validation, S.Y.; investigation, S.Y., A.N., K.Y., K.K., M.M., T.A., T.H., H.F. and T.K.; writing—original draft preparation, S.Y.; writing—review and editing, S.Y., A.N., K.Y., K.K., M.M., T.A., T.H., H.F. and T.K.; visualization, S.Y.; supervision, S.Y.; project administration, S.Y.; funding acquisition, S.Y. All authors have read and agreed to the published version of the manuscript.

Funding: This work was partially supported by the Fujimori Science and Technology Foundation. The authors express their gratitude to Nippon Zeon Corporation for the gift of the fluorinated starting substance, i.e., octafluorocyclopentene.

Institutional Review Board Statement: Not applicable.

Informed Consent Statement: Not applicable.

Data Availability Statement: Data is contained within the article or Supplementary Materials.

Conflicts of Interest: The authors declare no conflict of interest.

References

1. Chan, N.N.M.Y.; Idris, A.; Abidin, Z.H.Z.; Tajuddin, H.A.; Abdullah, Z. White light employing luminescent engineered large (mega) Stokes shift molecules: A review. *RSC Adv.* **2021**, *11*, 13409–13445. [CrossRef]
2. Holden, L.; Burke, C.S.; Cullinane, D.; Keyes, T.E. Strategies to promote permeation and vectorization, and reduce cytotoxicity of metal complex luminophores for bioimaging and intracellular sensing. *RSC Chem. Biol.* **2021**, *2*, 1021–1049. [CrossRef]
3. Ansari, A.A.; Thakur, V.K.; Chen, G. Functionalized upconversion nanoparticles: New strategy towards FRET-based luminescence bio-sensing. *Coord. Chem. Rev.* **2021**, *436*, 213821. [CrossRef]
4. Tang, M.C.; Chan, M.Y.; Yam, V.W.W. Molecular design of luminescent gold(III) emitters as thermally evaporable and solution-processable organic light-emitting device (OLED) materials. *Chem. Rev.* **2021**, *121*, 7249–7279. [CrossRef] [PubMed]
5. Bispo-Jr, A.G.; Saraiva, L.F.; Lima, S.A.M.; Pires, A.M.; Davolos, M.R. Recent prospects on phosphor-converted LEDs for lighting, displays, phototherapy, and indoor farming. *J. Lumines.* **2021**, *237*, 118167. [CrossRef]
6. Zhang, H.; Zhang, H.; Pan, A.; Yang, B.; He, L.; Wu, Y. Rare earth-free luminescent materials for WLEDs: Recent progress and perspectives. *Adv. Mater. Technol.* **2021**, *6*, 2000648. [CrossRef]
7. Kim, H.S.; Park, S.R.; Suh, M.C. Concentration quenching behavior of thermally activated delayed fluorescence in a solid film. *J. Phys. Chem. C* **2017**, *121*, 13986–13997. [CrossRef]
8. Birks, J.B. *Photophysics of Aromatic Molecules*; Birks, J.B., Ed.; Wiley: London, UK, 1970.
9. Thomas, S.W.; Joly, G.D.; Swager, T.M. Chemical sensors based on amplifying fluorescent conjugated polymers. *Chem. Rev.* **2007**, *107*, 1339–1386. [CrossRef] [PubMed]
10. Jenekhe, S.A.; Osaheni, J.A. Excimers and exciplexes of conjugated polymers. *Science* **1994**, *265*, 765–768. [CrossRef]
11. Han, T.; Yan, D.; Wu, Q.; Song, N.; Zhang, H.; Wang, D. Aggregation-induced emission: A rising star in chemistry and materials science. *Chin. J. Chem.* **2021**, *39*, 677–689. [CrossRef]
12. Zhao, Z.; Zhang, H.; Lam, J.W.Y.; Tang, B.Z. Aggregation-induced emission: New vistas at the aggregate level. *Angew. Chem. Int. Ed.* **2020**, *59*, 9888–9907. [CrossRef]
13. Leung, N.L.C.; Xie, N.; Yuan, W.; Liu, Y.; Wu, Q.; Peng, Q.; Miao, Q.; Lam, J.W.Y.; Tang, B.Z. Restriction of intramolecular motions: The general mechanism behind aggregation-induced emission. *Chem. Eur. J.* **2014**, *20*, 15349–15353. [CrossRef]
14. Li, M.; Niu, Y.; Zhu, X.; Peng, Q.; Lu, H.Y.; Xia, A.; Chen, C.F. Tetrahydro[5]helicene-based imide dyes with intense fluorescence in both solution and solid state. *Chem. Commun.* **2014**, *50*, 2993–2995. [CrossRef]
15. Lei, Y.; Liu, Q.; Dong, L.; Cai, Z.; Shi, J.; Zhi, J.; Tong, B.; Dong, Y. The dual-state luminescent mechanism of 2,3,4,5-Tetraphenyl-1H-pyrrole. *Chem. Eur. J.* **2018**, *24*, 14269–14274. [CrossRef]
16. Qiu, Q.; Xu, P.; Zhu, Y.; Yu, J.; Wei, M.; Xi, W.; Feng, H.; Chen, J.; Qian, Z. Rational design of dual-state emission luminogens with solvatochromism by combining a partially shared donor-acceptor pattern and twisted structures. *Chem. Eur. J.* **2019**, *25*, 15983–15987. [CrossRef] [PubMed]
17. Xu, Y.; Ren, L.; Dang, D.; Zhi, Y.; Wang, X.; Meng, L. A strategy of “Self-Isolated Enhanced Emission” to achieve highly emissive dual-state emission for organic luminescent materials. *Chem. Eur. J.* **2018**, *24*, 10383–10389. [CrossRef] [PubMed]
18. Wang, Y.; Pan, X.; Peng, Z.; Zhang, Y.; Liu, P.; Cai, Z.; Tong, B.; Shi, J.; Dong, Y. A “Turn-On” fluorescent chemosensor with the aggregation-induced emission characteristics for high-sensitive detection of Ce ion. *Sens. Actuators B* **2018**, *267*, 351–356. [CrossRef]
19. Zhang, Y.; Jiao, P.C.; Xu, H.B.; Tang, M.J.; Yang, X.P.; Huang, S.; Deng, J.G. Switchable sensitizers stepwise lighting up lanthanide emissions. *Sci. Rep.* **2015**, *5*, 9335. [CrossRef] [PubMed]
20. Kumar, S.; Singh, P.; Kumar, P.; Srivastava, R.; Pal, S.K.; Ghosh, S. Exploring an emissive charge transfer process in zero-twist donor-acceptor molecular design as a dual-state emitter. *J. Phys. Chem. C* **2016**, *120*, 12723–12733. [CrossRef]
21. Zhou, J.; Huang, M.; Zhu, X.; Wan, Y. One-pot synthesis of dual-state emission (DSE) luminogens containing the V-shape furo[2,3-b]furan scaffold. *Chin. Chem. Lett.* **2021**, *32*, 445–448. [CrossRef]
22. Yamada, S.; Nishizawa, A.; Morita, M.; Hosokai, T.; Okabayashi, Y.; Agou, T.; Hosoya, T.; Kubota, T.; Konno, T. Synthesis and characterization of bent fluorine-containing donor-p-acceptor molecules as intense luminophores with large Stokes shifts. *Org. Biomol. Chem.* **2019**, *17*, 6911–6919. [CrossRef]
23. CrysAlisPro 1.171.39.43a. Rigaku Oxford Diffraction, Rigaku Corporation: Akishima, Japan, 2015. Available online: <https://www.rigakuxrayforum.com/> (accessed on 30 September 2021).
24. Sheldrick, G.M. SHELXT—Integrated space-group and crystal-structure determination. *Acta Cryst. Sect. A Found. Adv.* **2015**, *71*, 3–8. [CrossRef]
25. Sheldrick, G.M. Crystal structure refinement with SHELXL. *Acta Cryst. Sect. C Struct. Chem.* **2015**, *71*, 3–8. [CrossRef]
26. Dolomanov, O.V.; Bourhis, L.J.; Gildea, R.J.; Howard, J.A.K.; Puschmann, H. OLEX2: A complete structure solution, refinement and analysis program. *J. Appl. Crystallogr.* **2009**, *42*, 339–341. [CrossRef]
27. Frisch, M.J.; Trucks, G.W.; Schlegel, H.B.; Scuseria, G.E.; Robb, M.A.; Cheeseman, J.R.; Scalmani, G.; Barone, V.; Petersson, G.A.; Nakatsuji, H.; et al. *Gaussian 16, Revision B.01*; Gaussian, Inc.: Wallingford, CT, USA, 2016.
28. Okuno, K.; Shigeta, Y.; Kishi, R.; Nakano, M. Non-empirical tuning of CAM-B3LYP functional in time-dependent density functional theory for excitation energies of diarylethene derivatives. *Chem. Phys. Lett.* **2013**, *585*, 201–206. [CrossRef]
29. Yanai, T.; Tew, D.P.; Handy, N.C. A new hybrid exchange-correlation functional using the Coulomb-attenuating method (CAM-B3LYP). *Chem. Phys. Lett.* **2004**, *393*, 51–57. [CrossRef]

30. Andzelm, J.; Kölmel, C.; Klamt, A. Incorporation of solvent effects into density functional calculations of molecular energies and geometries. *J. Chem. Phys.* **1995**, *103*, 9312–9320. [[CrossRef](#)]
31. Barone, V.; Cossi, M. Quantum calculation of molecular energies and energy gradients in solution by a conductor solvent model. *J. Phys. Chem. A* **1998**, *102*, 1995–2001. [[CrossRef](#)]
32. Cossi, M.; Rega, N.; Scalmani, G.; Barone, V. Energies, structures, and electronic properties of molecules in solution with the C-PCM solvation model. *J. Comput. Chem.* **2003**, *24*, 669–681. [[CrossRef](#)] [[PubMed](#)]
33. Grad, J.; Yan, Y.J.; Mukamel, S. Time-dependent self-consistent field approximation for semiclassical dynamics using Gaussian wavepackets in phase space. *Chem. Phys. Lett.* **1987**, *134*, 291–295. [[CrossRef](#)]
34. Makri, N. Time-dependent self-consistent field approximation with explicit two-body correlations. *Chem. Phys. Lett.* **1990**, *169*, 541–548. [[CrossRef](#)]
35. Bondi, A. van der Waals volumes and radii. *J. Phys. Chem.* **1964**, *68*, 441–451. [[CrossRef](#)]
36. Mataga, N.; Kaifu, Y.; Koizumi, M. The solvent effect on fluorescence spectrum, change of solute-solvent interaction during the lifetime of excited solute molecule. *Bull. Chem. Soc. Jpn.* **1955**, *28*, 690–691. [[CrossRef](#)]
37. Mataga, N.; Kaifu, Y.; Koizumi, M. Solvent effects upon fluorescence spectra and the dipole moments of excited molecules. *Bull. Chem. Soc. Jpn.* **1956**, *29*, 465–470. [[CrossRef](#)]